BNL-107401-2015-JA

Pseudo-rotational epitaxy of self-assembled OTS monolayers on sapphire (0001)

H.-G. Steinrück,[1] A. Magerl,[1] M. Deutsch,[2] and B.M. Ocko[3,*]

[1] *Crystallography and Structural Physics, University of Erlangen-Nürnberg, 91058 Erlangen, Germany*
[2] *Physics Dept. & Institute of Nanotechnology, Bar-Ilan University, Ramat-Gan 52900, Israel*
[3] *Condensed Matter Physics & Materials Science Dept., Brookhaven National Lab, Upton, NY 11973, USA*

The structure of octadecyltrichlorosilane (OTS) self-assembled monolayers (SAMs) on sapphire (0001) was studied by Å-resolution surface specific x-ray scattering methods. The monolayer was found to consist of three sub-layers where the outmost layer corresponds to vertically oriented, closely packed alkyl tails. Laterally, the monolayer is hexagonally packed and exhibits pseudo-rotational epitaxy to the sapphire, manifested by a broad scattering peak at zero relative azimuthal rotation, with long powder-like tails. The lattice mismatch of $\sim 1-3\%$ to the sapphire's and the different length scale introduced by the lateral Si-O-Si bonding prohibit positional epitaxy. However, the substrate induces an intriguing increase in the crystalline coherence length of the SAM's powder-like crystallites when rotationally aligned with the sapphire's lattice. The increase is shown to correlate well with the rotational dependence of the separation of corresponding substrate-monolayer lattice sites.

Self-Assembled Monolayers (SAMs) have been intensely studied since their inception in the 1980s [1, 2]. Their many applications range from organic field-effect transistors [3], photovoltaic devices [4], biosensors [5] and enzyme electrodes [6] to adhesion promoters [7] and lubricants [8]. For basic science, they are intriguing model systems for the study of self-organization in two-dimensional matter under the complex interplay of van der Waals (vdW), covalent and electrostatic interactions [2]. The most widely studied SAMs are alkylsilanes on the native oxide of silicon [1]. However, being amorphous, the native oxide can not promote lateral ordering, or tune the structure, of the SAM by epitaxy. The SAM's observed hexagonal order originates, therefore, from the chain-chain vdW interaction. However, the difference in the chain-chain spacing and the length of an intralayer Si-O-Si oligomer [9] frustrates the lateral packing and yields a reduced crystalline coherence length, as we discuss below.

Here we explore how a highly ordered substrate, single-crystal sapphire Al_2O_3 (0001), affects the structure of an OTS SAM. Surface-specific x-ray scattering measurements yield a detailed sub-molecular-resolution determination of the SAM's structure, hitherto studied on sapphire only by low resolution, or macroscopic, methods like AFM, XPS, and ellipsometry [10]. The ultra-smooth sapphire enables high resolution x-ray reflectivity measurements of the SAM's vertical structure, revealing a monolayer consisting of a stack of three distinct sub-layers. Laterally, the SAM consists of vertically aligned molecules, with closely-packed, fully extended alkyl chains exhibiting hexagonal order, as does the underlying sapphire substrate, but with a lattice mismatch of 1% at room temperature, increasing to 3% at $T = 60$ °C. A novel type of epitaxial relation between the two lattices is found, where the underlying sapphire lattice imparts to the SAM's crystallites a preferred azimuthal orientation with a large angular width and powder-like tails. In addition, the SAM's crystalline coherence length, ξ, is found to increase as the relative azimuthal rotation angle, φ, decreases to zero. This increase is shown to correlate well with the angular dependence of the separation of corresponding sites in the monolayer and substrate lattices. We now discuss these results in detail.

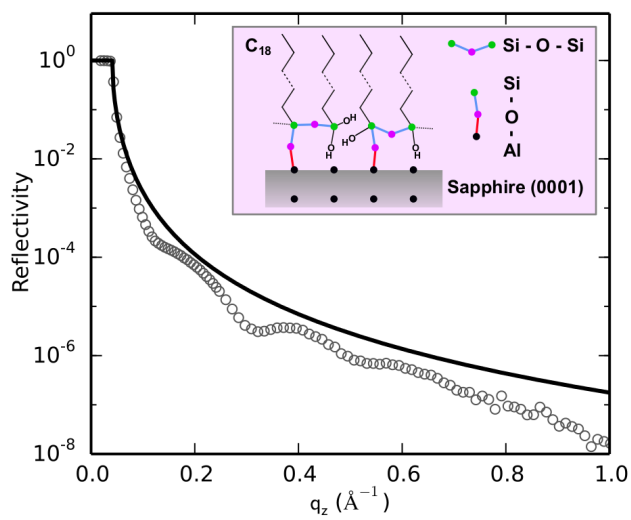

FIG. 1. Measured (symbols) x-ray reflectivity curve $R(q_z)$ for an OTS-SAM on sapphire and the corresponding Fresnel $R_F(q_z)$ curve (line) of an ideally flat and abrupt sapphire surface. Inset: schematic representation of the OTS-SAM monolayer on a sapphire substrate. The substrate-OTS bonds and the OTS-OTS cross links are shown, respectively, as red and blue lines.

The SAM's vertical structure, shown schematically in the inset of Fig. 1, was determined by x-ray reflectivity (XRR) [11] using a setup described previously [3]. XRR measures $R(q_z)$, the reflected intensity fraction of

an x-ray beam of wavelength λ incident on the SAM at a grazing angle α. $q_z = (4\pi/\lambda)\sin\alpha$ is the surface-normal scattering vector. The measured XRR is shown in Fig. 1 along with the Fresnel XRR of an ideally smooth and abrupt interface, $R_F(q_z)$. Note the large measurable range, up to $q_z \sim 1$ Å^{-1}, yielding high spatial resolution. This is due to the very low roughness of the sapphire, $\sigma_0 \approx 2$ Å. The Kiessig-like fringes [11] observed in Fig. 1 are due to interference of rays reflected from the SAM's top and bottom interfaces, and yield an estimate of the SAM's thickness, $d = 2\pi/(\Delta q_z) = 33$ Å, based on the fringes' periodicity, $\Delta q_z \approx 0.19$ Å^{-1}. This d is significantly larger than the 24-26 Å calculated for the molecular length [12, 13], and the 23-27 Å refined from XRR measurements for the same SAM on native SiO_2 [13–15]. To elucidate the origin of this large discrepancy, and the SAM's internal structure, a detailed modeling of the XRR's surface-normal structure is required.

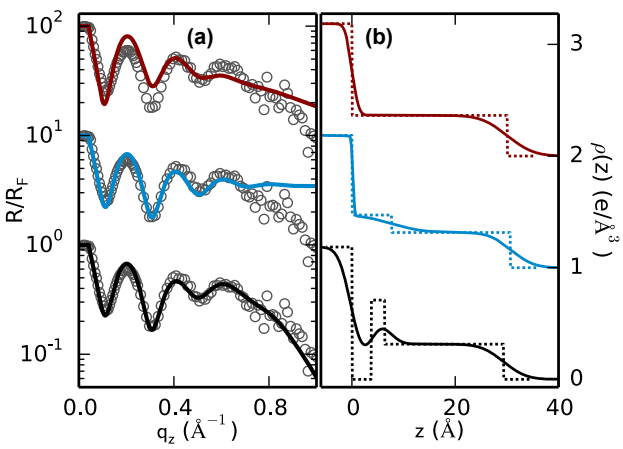

FIG. 2. (a) Fresnel-normalized measured XRR (symbols) of OTS on sapphire and the corresponding model fits (lines) for 1- (brown), 2- (blue) and 3-slab (black) models, vertically spaced for clarity. (b) The same-color fit-derived electron density profiles with (solid lines) and without (doted lines) surface roughness.

Following previous studies [16, 17], the SAM's surface-normal electron density, $\rho(z)$, is modeled by a stack of 1, 2 or 3 "slabs", each of uniform, but variable, electron density, ρ_i, and thickness, d_i. A Gaussian roughness of width σ_i is assumed at each interface. An additional slab with $d_0 = \infty$, $\rho_0 = 1.18$ e/Å^3, and roughness σ_0 represents the sapphire. This model $\rho_m(z)$ is then used to least-squares fit the measured XRR curves by the Abeles transfer matrix method, as implemented in the MOTOFIT package [18]. The fit yields the best values for the model-defining parameters: ρ_i, d_i and σ_i.

Fig. 2(a) shows the best fits in solid lines, and the corresponding $\rho(z)$ profiles, in the same colors, - in (b). A 1-slab model, which accounted well for octadecanol monolayers on sapphire [17], clearly provides here a poor fit. A 2-slab model, used successfully for OTS SAMs on native SiO_2 [14, 19], provides a better fit. However, the resultant SAM thickness, 30.7 Å, is significantly larger than the extended molecule's length, 26-27 Å, and the refined substrate roughness, 0.3 Å, is unphysically small. A 3-slab model yields a near-perfect fit, with physically-realistic parameter values. Here the top slab (3) represents the alkyl chains, the middle slab (2) - the high-density cross-linking region of lateral Si-O-Si bonds [9], and the bottom slab (1) - the substrate-adjacent low density region of the headgroup-substrate bonds (Fig. 1, inset). As the fit is only weakly sensitive to the values of ρ_1 and ρ_2, they were fixed, respectively, to zero and the density of silicon, $\rho \approx 0.7$ e/Å^3. The thickness and density of slab 3 were also fixed at values calculated for close-packed, vertically-aligned, extended alkyl chains, 23 Å and 0.32 e/Å^3, respectively. Furthermore, the roughnesses of the sapphire and slabs 1 and 2 were fixed at 2 Å. The thicknesses of slabs 1 and 2 and the roughness of slab 3 were then fitted, yielding $d_1 = 3.7 \pm 0.1$ Å, $d_2 = 2.7 \pm 0.1$ Å and $\sigma_3 = 3.5 \pm 0.1$ Å. The total SAM thickness, 29.4 Å, is now closer to the 27 Å measured thickness of OTS on native SiO_2 [14], and the extended molecular length derived from the 1.27 Å molecular-axis-projected C-C distance [20]. The few Å discrepancy may in part reflect both incomplete bonding of the silane group with the sapphire and the lattice corrugation from the incommensurate lattice.

The SAM's lateral order was explored by grazing-incidence diffraction (GID). Here the x-rays' incidence angle α is kept small and the detector scanned out of the reflection plane by an angle 2θ, yielding a lateral diffraction vector $q_r \approx (4\pi/\lambda)\sin\theta$, which probes the surface-parallel order [11]. Using a vertically-aligned linear detector, the q_z distribution of the scattered intensity at each q_r, known as a Bragg rod (BR), was measured simultaneously. The SAM's epitaxy was explored by GID scans at different azimuthal substrate rotations, φ, relative to the sapphire's $(10\overline{1}0)$ peak.

Fig. 3(a) shows the measured (q_r, q_z) intensity map, the BR, for the single GID peak found. The single peak indicates a lateral hexagonal molecular order within the SAM. The absence of higher order peaks is typical of rotator phases [16, 21, 22], and is due to the molecular form factor's fast fall-off with q_r. The peaking of the BR's intensity in Fig. 3(a) at $q_z \approx 0$ Å^{-1} indicates vertically-aligned molecules [16], although a small, 1-2°, tilt can not be ruled out. As the peaks' q_r-position is φ-independent (see below), this φ-distribution attests to a non-zero GID peak intensity over a broad range of φ positions, i.e. to a powder-like behavior of the OTS monolayer. This point, impacting on the epitaxy issue, will be further discussed in below. The broad azimuthal distribution from the SAM (red circles) is in contrast to the sharp, resolution-limited peak from the uncoated substrate (open circles). The SAM is predominately ro-

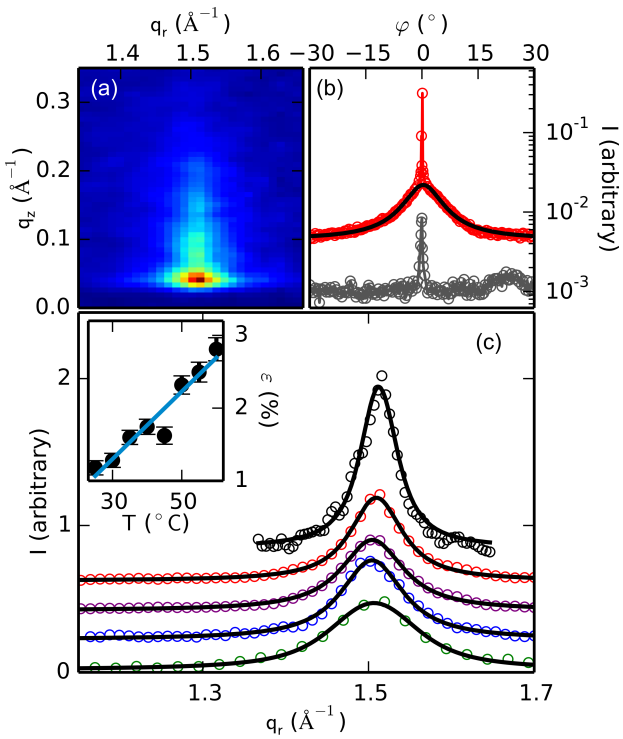

FIG. 3. (a) Grazing incidence X-ray diffraction intensity map in the (q_r, q_z) plane showing a Bragg rod, originating in the OTS monolayer. (b) Measured intensity variation (red line) upon azimuthal substrate rotation, φ, at $q_r = 1.505 \pm 0.010$ Å^{-1} and its Lorentzian fit (thick black line). A bare substrate scan is also shown (black line). (c) Measured (symbols) GID peaks at different azimuthal rotations, and their Lorentzian fits (lines), for ϕ =0.1° (black), 1° (red), 2° (purple), 3° (blue), and 20° (green). Curves are spaced vertically for clarity. Inset: SAM-sapphire lattice constant mismatch, ε, vs. temperature T.

tationally aligned with the sapphire since both azimuthal (φ) scans peak at the same position. Note that the sapphire peak shown in Fig. 3(b) is weak since the q_r position where the φ scan was measured is that of the SAM's peak, which is somewhat smaller than the q_r of the sapphire peak.

The SAM's azimuthal scattering peak in Fig. 3(b) is well fitted (black solid line) by a Lorentzian profile of a half width at half maximum of $(10.0 \pm 0.2)°$, (excluding the very sharp sapphire peak at $\varphi = 0$), and a constant intensity at large φ. The constant term is suggestive of powder-like behavior and further support is provided by the φ-independent q_r peaks position (see below).

The q_r widths of the peaks shown in Fig. 3(c) appear to exhibit φ-dependent behavior. To quantify this observation, the measured curves were fitted by an intrinsic Lorentzian lineshape [14], $I(q_r) = (I_0\kappa_r/2\pi)/\left[(q_r - q_0)^2 + (\kappa_r/2)^2\right]$, convoluted with the measured Gaussian resolution function. The fits (lines)

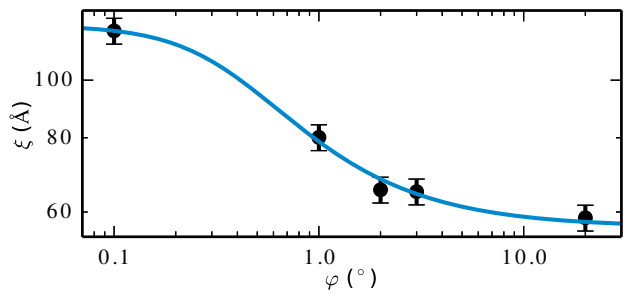

FIG. 4. (a) Crystalline coherence length, ξ, of the OTS's crystallites as a function of the substrate's azimuthal rotation φ from the in-plane sapphire peak. The line is the fit to the model discussed in the text.

demonstrate the φ-independence of the peak position at $q_0 = 1.505 \pm 0.010$ Å^{-1}. The corresponding lattice constant, $a_{OTS} = 4\pi/(\sqrt{3}q_0) = 4.82$ Å, is $\sim 1\%$ larger than the sapphire's $a_{sap} = 4.76$ [17], which prohibits a perfect epitaxy between the monolayer and the substrate. The 4.82 Å lattice constant is very close to its value for OTS on the the native SiO_2 surface [22] and for surface frozen alkane monolayers [23], suggesting that the spacing originates from the chain-chain vdW interactions. In contrast, a Si-O-Si oligomer gives rise to a spacing of 3.3 Å [24], shorter than a_{OTS}, and on the native SiO_2 surface it has been suggested that this difference is the origin of the short crystalline coherence length [9], discussed next.

The φ-dependent intrinsic widths, κ_r, also obtained from the fits, yield the crystalline coherence length, ξ, of the SAM's 2D crystallites through the Debye-Scherrer formula, $\xi \approx (0.9 \cdot 2\pi)/\kappa_r$ [25, 26]. $\xi(\varphi)$, shown in Fig 4(a), varies from (120 ± 6) Å at $\varphi = 0.1°$ to (60 ± 5) Å at $\varphi = 20°$. The last value agrees well with the $\xi \approx 65$ Å for OTS on native SiO_2, calculated from the measurements of Tidswell et al. [22]. This ξ is, however, φ-independent due to the amorphous nature of the underlying oxide.

To determine the SAM's thermal evolution, GID measurements were repeated for temperatures up to 60 °C at $\varphi = 20°$. While κ_r, and hence ξ, are found to be T-independent, the lattice mismatch, $\varepsilon = (a_{OTS} - a_{sap})/a_{sap}$, shown in the inset to Fig. 3(c), increases linearly from 1.2% at 25 °C to 2.8% at 60 °C, yielding an areal expansion coefficient $\alpha_A = (\mathrm{d}A/\mathrm{d}T)/A = 0.94 \times 10^{-3}$ K^{-1} where A is the OTS's molecular area. Interestingly, the same α_A is obtained for OTS on native SiO_2 [27] despite the absence of preferred orientational order. The absence of cross-linking in purely vdW-bound organic monolayers of alkanes, alcohols and fatty-acids, supported either on their own melt or on liquid mercury [23, 27] results in a 40%-100% larger α_A than that found here.

Turning now to the subject of substrate-monolayer

epitaxy, we note that the structural relations between identical-symmetry, but different lattice-constant, substrate and overlayer have been studied extensively [28, 29]. Several theoretical approaches have been developed to account for epitaxy in theses systems [30–34]. However, no single theoretical model has emerged as yet for describing the rich epitaxial behavior experimentally observed for overlayers, and some important systems, e.g. halogens and alkalis on metals, are still not understood [33, 35]. In hexagonal systems, e.g. atomic monolayers on graphite [36] and on single-crystal metal facets [35, 37]), and graphene on metals [29, 38, 39], the monolayer-substrate lattice mismatch relaxes by a combination of compression and relative azimuthal rotation of the substrate and overlayer lattices. The rotation angle depends on the corrugation potential landscape of the substrate, the substrate-monolayer interaction strength, and the elastic properties of the monolayer. These factors induce in many systems rotation angles in the substrate's symmetry, or non-symmetry, azimuthal directions [30, 31, 35]. Moreover, the rotation angles are few, and sharply defined. In contrast, Figs. 3 and 4 demonstrate that here a GID peak is observed for all azimuthal rotations φ. Our monolayer exhibits, therefore, a 2D-powder-like behavior, with crystallite rotations spanning the measured $-30° \leq \varphi \leq 30°$ range. This non-discret, broad range, azimuthal orientation distribution, and the φ-independence of a_{OTS}, which demonstrates that a crystallite rotation is not accompanied by an elastic lattice relaxation, imply that the monolayer's lattice does not lock into that of the underlying substrate even though the lattice mismatch is small, 1.2% only. Thus, the epitaxy is very weak. Nevertheless, it is still sufficiently strong to induce an increase in ξ for crystallites closely aligned with the substrate's lattice, i.e. $\varphi \approx 0$.

The φ dependence of ξ, shown in Fig. 4, can be rationalized as follows. For large φ an intrinsic, φ-independ $\xi_0 \approx 60$ Å is observed, identical with that observed for OTS on native amorphous SiO_2 [22]. ξ_0 is likely determined by the vdW interaction of the OTS alkyl tails and the lateral Si-O-Si bonds of the OTS headgroups. In addition, Fig. 4 shows that ξ must include a term which increases with decreasing φ, presumably as a result of the increasing rotational epitaxy to the substrate. This term can be obtained by a simple geometrical argument as follows. Assume two identical, overlapping hexagonal lattices, a crystal and an overlayer, with an interface-normal rotation axis through a coinciding lattice site. Expand now the overlayer lattice by a multiplicative factor of $(1+\varepsilon)$, and rotate it azimuthally by an angle φ. Simple geometry shows that this will cause an overlayer site some distance $\hat{\xi}$ from the axis to move away from its initially coinciding substrate site by a distance $\delta = \hat{\xi}\sqrt{\varepsilon^2 + 4(1+\varepsilon)\sin^2(\varphi/2)}$. Once δ exceeds some critical value, η, (which may be a fraction of, or the full, nearest neighbor distance in the bottom lattice) the two lattice sites may be considered to cease being epitaxially related to each other. However, all overlayer sites at distances shorter than $\hat{\xi}$ from the rotation axis will have $\delta < \eta$ and hence remain epitaxial to the substrate. Thus, η imposes a φ-dependent limit, $\eta/\sqrt{\varepsilon^2 + 4(1+\varepsilon)\sin^2(\varphi/2)}$, on the radius $\hat{\xi}$ inside which the two lattices may be considered epitaxially related. Making now the reasonable assumption that epitaxy causes the increase in the overlayer's crystalline coherence length ξ over ξ_0, we can write $\xi = \xi_0 + \hat{\xi} = \xi_0 + \eta/\sqrt{\varepsilon^2 + 4(1+\varepsilon)\sin^2(\varphi/2)}$. For a more realistic, non-abrupt loss of epitaxy with increasing $\hat{\xi}$, contributions to this loss from crystal defects, possible very small ε variation upon rotation, etc., ξ can be generalized to $\xi = \xi_0 + \eta/\sqrt{\varepsilon^2 + 4B(1+\varepsilon)\sin^2(\varphi/2)}$, where B is a fit parameter. In spite of its simplicity this ad-hoc expression seems to capture the main features of the φ-variation of ξ, as demonstrated by its good fit to the, admittedly few, measured ξ values, shown in Fig. 4, which yields $\xi_0 = 57$ Å, $\eta = 0.87$ Å, and $B = 4.5$. This said, it is clear that a more physical, molecular-level, model which accounts for the disorder inducing Si-O-Si bonds is required to fully account for $\xi(\varphi)$ and the unusual type of epitaxy found here, which we denote as pseudo-rotational epitaxy. Such theory should take into consideration all lateral molecular interactions within the overlayer, and those between the overlayer and the substrate's corrugation potential.

The study presented here provides an unprecedentally detailed, Å-resolution, description of the surface-normal and surface-parallel structure of an OTS monolayer self-assembled on an ordered sapphire substrate. XRR shows the monolayer to be thicker by ~ 2.5 Å than the extended molecular length and this may reflect both the incomplete bonding of the silane group with the sapphire and the lattice corrugation from the incommensurate lattice. GID measurements demonstrate that the OTS monolayer consists of surface-normal-aligned molecules, ordered hexagonally, as does the underlying sapphire (0001) facet. However, the monolayer's $\sim 1\%$ larger lattice constant prevents perfect epitaxy between the two lattices. In previously studied similar systems the mismatch relaxes by an azimuthal rotation of the two lattices by a single (or few) sharply-defined angles [30, 33, 34], or, for a small, few-percent, mismatch, remain unrotated, in spite of the energy cost of the resultant strain [32, 35]. Here, the monolayer exhibits powder-like features and a rotation-independent lattice constant, implying a weak epitaxial relation, which causes only an enhancement of the azimuthal orientation of crystallites, and of the crystalline coherence length ξ, as $\varphi = 0$ is approached. The increase in ξ is shown to correlate quantitatively with the separation of corresponding lattice sites in the substrate and the monolayer. This constitutes an intermediate type of

epitaxy, pseudo-rotational epitaxy, where no positional or rotational epitaxy exist between substrate and monolayer, yet the monolayer's crystalline properties, ξ and crystallite orientation in this case, are influenced by epitaxy to the substrate. To our knowledge, such behavior has not been hitherto reported, and we hope that this study will lead to theoretical treatments of such systems.

Financial support through the DFG research unit 1878, "Functional Molecular Structures on Complex Oxide Surfaces", is gratefully acknowledged. We thank Alexei Tkachenko (BNL) for important discussions and the US-Israel Binational Science Foundation, Jerusalem, for support. Work at BNL is supported by the Division of Materials Sciences (DOE) under contract DE-AC02-76CH0016.

* E-mail: ocko@bnl.gov

[1] C. D. Bain, E. B. Troughton, Y. T. Tao, J. Evall, G. M. Whitesides, and R. G. Nuzzo, J. Am. Chem. Soc. **111**, 321 (1989); J. Sagiv, *ibid.* **102**, 92 (1980).

[2] S. Onclin, B. J. Ravoo, and D. N. Reinhoudt, Angew. Chem. **44**, 6282 (2005); F. Schreiber, Prog. Surf. Sci. **65**, 151 (2000); D. K. Schwartz, Ann. Rev. Phys. Chem. **52**, 107 (2001); A. Ulman, Chem. Rev. **96**, 1533 (1996).

[3] M. Halik and A. Hirsch, Adv. Mat. **23**, 2689 (2011); S. G. J. Mathijssen et al., Nature Tech. **4**, 674 (2009); T. Schmaltz et al., Adv. Mat. **25**, 4511 (2013); E. C. P. Smits et al., Nature **455**, 956 (2008).

[4] R. J. Kline, M. D. Mcgehee, and M. F. Toney, Nature Mat. **5**, 222 (2006).

[5] J. N. Anker, W. P. Hall, O. Lyandres, N. C. Shah, J. Zhao, and R. P. Van Duyne, Nature Mat. **7**, 442 (2008); N. K. Chaki and K. Vijayamohanan, Biosens. Bioelect. **17**, 1 (2002).

[6] J. J. Gooding and D. B. Hibbert, TRAC-Trends Aanal. Chem. **18**, 525 (1999).

[7] D. G. Kurth and T. Bein, Langmuir **11**, 3061 (1995).

[8] X. D. Xiao, J. Hu, D. H. Charych, and M. Salmeron, Langmuir **12**, 235 (1996).

[9] R. Maoz, S. Matlis, E. DiMasi, B. Ocko, and J. Sagiv, Nature **384**, 150 (1996); R. Maoz, J. Sagiv, D. Degenhardt, H. Möhwald, and P. Quint, Supramol. Sci. **2**, 9 (1995).

[10] L. N. Mitchon and J. M. White, Langmuir **22**, 6549 (2006).

[11] P. S. Pershan and M. L. Schlossman, *Liquid Surfaces and Interfaces: Synchrotron X-ray Methods* (cambridge University Press, Cambridge, UK, 2012); M. Deutsch and B. M. Ocko, *Encyclopedia of Applied Physics*, edited by G. L. Trigg, Vol. 23 (VCH, New York, USA, 1998); M. Tolan, *X-ray scattering from soft matter thin films* (Springer, Berlin,Germany, 1999); J. Als-Nielsen and D. McMorrow, *Elements of Modern X-ray Physics* (Wiely, New York, USA, 2001).

[12] T. Koga, K. Honda, S. Sasaki, O. Sakata, and A. Takahara, Langmuir **23**, 8861 (2007).

[13] T. Ishizaki, N. Saito, S. H. Lee, and O. Takai, Nanotech. **19** (2008).

[14] I. M. Tidswell, B. M. Ocko, P. S. Pershan, S. R. Wasserman, G. M. Whitesides, and J. D. Axe, Phys. Rev. B **41**, 1111 (1990); M. Mezger et al., J. Chem. Phys. **128** (2008).

[15] K. Kojio, A. Takahara, K. Omote, and T. Kajiyama, Langmuir **16**, 3932 (2000).

[16] B. M. Ocko, X. Z. Wu, E. B. Sirota, S. K. Sinha, O. Gang, and M. Deutsch, Phys. Rev. E **55**, 3164 (1997).

[17] B. M. Ocko, H. Hlaing, P. N. Jepsen, S. Kewalramani, A. Tkachenko, D. Pontoni, H. Reichert, and M. Deutsch, Phys. Rev. Lett. **106**, 137801 (2011); L. Tamam, B. M. Ocko, H. Reichert, and M. Deutsch, *ibid.* **106**, 197801 (2011).

[18] F. Abeles, J. Phys. Radium **11**, 307 (1950); A. Nelson, J. App. Crystall. **39**, 273 (2006).

[19] A. G. Richter, M. K. Durbin, C. J. Yu, and P. Dutta, Langmuir **14**, 5980 (1998).

[20] D. M. Small, *The Physical Chemistry of Lipids* (Plenum, New York, USA, 1986).

[21] V. M. Kaganer, H. Mohwald, and P. Dutta, Rev. Mod. Phys. **71**, 779 (1999); I. Kuzmenko, V. M. Kaganer, and L. Leiserowitz, Langmuir **14**, 3882 (1998).

[22] I. M. Tidswell, T. A. Rabedeau, P. S. Pershan, S. D. Kosowsky, J. P. Folkers, and G. M. Whitesides, J. Chem. Phys. **95**, 2854 (1991).

[23] B.M. Ocko et al., Phys. Rev. E **63**, 032602 (2001).

[24] R. C. Weast, *CRC Handbook of Chemistry and Physics*, 54th ed. (CRC Press, New York, USA, 1974).

[25] L. Tamam, H. Kraack, E. Sloutskin, B. M. Ocko, and M. Deutsch, Phys. Rev. B **85**, 205449 (2012).

[26] A. Guinier, *X-Ray Diffraction* (Freeman, San Francisco, USA, 1963).

[27] H. G. Steinrück, M. Deutsch, B. M. Ocko, and A. Magerl, To be published. E. Sloutskin, H. Kraack, B. Ocko, J. Ellmann, M. Moller, P. Lo Nostro, and M. Deutsch, Langmuir **18**, 1963 (2002); H. Kraack, B. M. Ocko, P. S. Pershan, E. Sloutskin, L. Tamam, and M. Deutsch, *ibid.* **20**, 5375 (2004); **20**, 5386 (2004).

[28] G. A. Somorjai, *Introduction to Surface Chemistry and Catalysis* (Wiley, New York, USA, 1994); Y. H. Wu, T. Yu, and Z. X. Shen, J. Appl. Phys. **108** (2010).

[29] J. Wintterlin and M.-L. Bocquet, Surf. Sci. **603**, 1841 (2009).

[30] J. P. McTague and A. D. Novaco, Phys. Rev. B **19**, 5299 (1979).

[31] F. Grey and J. Bohr, Europhys. Lett. **18**, 717 (1992).

[32] H. Shiba, J. Phys. Soc. Japan **46**, 1852 (1979); **48**, 211 (1980).

[33] A. C. Hillier and M. D. Ward, Phys. Rev. B **54**, 14037 (1996).

[34] A. Tkatchenko, Phys. Rev. B **74**, 035428 (2006).

[35] G. Leatherman and R. Diehl, Phys. Rev. B **53**, 4939 (1996).

[36] K. L. D'Amico, D. E. Moncton, E. D. Specht, R. J. Birgeneau, S. E. Nagler, and P. M. Horn, Phys. Rev. Lett. **53**, 2250 (1984).

[37] O. Magnussen, Chem. Rev. **102**, 679 (2002); O. M. Magnussen, B. M. Ocko, R. R. Adzic, and J. X. Wang, Phys. Rev. B **51**, 5510 (1995); B. M. Ocko, G. M. Watson, and J. Wang, J. Chem. Phys. **98**, 897 (1994).

[38] J. Coraux, A. T. N'Diaye, C. Busse, and T. Michely, nano Lett. **8**, 565 (2008).

[39] D. Franz et al., Phys. Rev. Lett. **110** (2013).